ISSN-P: 2807-5987

Preparation, Characterization and Fluorescence Spectroscopic Studies of Polyacrylic Acid Mixed with Different Ratios of Silver Nanoparticles/Rhodamine B

W. Madani[a] and R. Seoudi[a, b]

[a] Department of Physics, College of Applied Science, Umm Al-Qura University, Makkah, Saudi Arabia

[b]Spectroscopy Department, Physics Division, NRC, Dokki, Cairo 12622, Egypt

ISSN-E: 26632806

ISSN-P: 2807-5987

Abstract

Silver nanoparticles (AgNPs) were prepared at 80^{O}C and various times using the chemical reduction method. Silver nanoparticles were mixed with rhodamine B (RhB) and blended with polyacrylic acid (PAA) to enhance the fluorescence spectra. The effects of preparation times on the surface plasmon resonance (SPR) were studied using UV-Vis spectroscopy. TEM measurements of the samples synthesized at 1, and 3 min confirmed the formation of AgNPs with an average size of 13 nm and 19 nm. In addition, the FTIR data showed that the bands that appeared at 1683 cm^{-1} and 1243 cm^{-1} of PAA were changed after mixing polyacrylic acid (PAA) with AgNPs/RhB due to the interaction between AgNPs and PAA through the C=O and C-O functional groups. The new high-intensity band at 560 nm and low at 408 in the UV-visible measurements of PAA were identified by RhB and AgNPs. The crystallization of PAA-doped by (RhB/AgNPs) was determined by X-ray diffraction. Fluorescence measurements from PAA blended indicated an emission band appeared between 587 nm and 440 nm for RhB, AgNPs with 13 nm and 19 nm, respectively. Peaks emission has a wavelength higher than the exciting wavelength, indicating the electronic transition from surface plasmon resonance of the nanoparticles and π-π* from RhB to PAA. PAA blended by AgNPs/RhB enhances the fluorescence spectra of the PAA.

Keywords: Silver nanoparticles; Dye doped polymer; FTIR; Fluorescence

ISSN-P: 2807-5987

الملخص

تم تحضير جسيمات الفضة النانوية (AgNPs) عند 80 درجة مئوية بأزمنة تحضير مختلفة باستخدام طريقة الاختزال الكيميائي. تم خلط جسيمات الفضة النانوية مع رودامين ب (RhB) وخلطها مع حمض البولي أكريليك (PAA) لتعزيز أطياف فلورية. تمت دراسة تأثير زمن تحضير جسيمات الفضة النانوية على رنين البلازمون السطحي (SPR) باستخدام جهاز التحليل الطيفي للأشعة المرئية وفوق البنفسجية. أكدت قياسات العينات بواسطة المجهر الإلكتروني النافذ(TEM) التي تم أخذها في الدقيقة الأولى و الدقيقة الثالثة من تكون جسيمات الفضة أن متزسط حجم هذه الجسيمات هو 13 نانومتر و 19 نانومتر، بالإضافة إلى ذلك ، أظهرت بيانات التحليل الطيفي بالأشعة تحت الحمراء (FTIR) تغيير في النطاقات التي ظهرت عند $1683\ cm^{-1}$ و $1243\ cm^{-1}$ لبوليمر حمض البولي أكريليك بعد التطعيم حمض بجزيئات الفضة النانوية / رودامين ب(RhB) بسبب التفاعل بين الجسيمات النانوية الفضية وحمض البولي أكريليك من خلال المجموعات الوظيفية C = O و C–O. كما تم تحديد نطاق جديد عالي الكثافة عند 560 نانومتر و منخفض الكثافة عند 408 نانومتر نتيجة قياس طيف الامتصاص للبوليمر المطعم بالرودامين ب و جسيمات الفضة النانوية بواسطة مطياف الاشعة المرئية و الأشعة الفوق البنفسجية. تم تحديد التبلور لحمض البولي أكريليك المطعم بواسطة (رودامين ب / جسيمات الفضة النانوية) عن طريق حيود الأشعة السينية. أشارت القياسات الفلورية (فلوروسينس) لحمض البولي أكريليك المطعم بالرودامين ب ، وجسيمات الفضة النانوية إلى ظهور نطاق انبعاث ما بين 587 نانومتر و 440 نانومتر لجسيمات الفضة النانوية عند حجم 13 نانومتر و 19 نانومتر ، على التوالي. قمم نطاقات الانبعاث لها أطوال موجية أعلى من الطول الموجي المثير ، مما يشير إلى الانتقال الإلكتروني من رنين البلازمون السطحي للجسيمات النانوية و $\pi-\pi$ * من رودامين ب إلى حمض البولي أكريليك. حمض البولي أكريليك الممزوج بجسيمات الفضة النانوية / رودامين ب يعزز الأطياف الفلورية لحمض البولي أكريليك.

الكلمات المفتاحية: جزيئات الفضة النانوية؛ بوليمر مطعم بالصبغة ؛ التحليل الطيفي بالأشعة تحت الحمراء؛ فلوروسينس

1.Introduction

Recently, metal nanoparticles have gained much interest, mainly due to their colorimetric characteristics (Oliveira, E., et al., 2015). Metal nanoparticles play an essential role in the electronic fields, nanolasers, optoelectronic devices, and fluorescing dye (Prakash, A., et al., 2019; Ning, S., et al., 2016; Wang, H., et al., 2005). There are more methods to prepare metal nanoparticles as biological (Gudikandula, K., & Charya Maringanti, S., 2016), physical (Prakash, A., et al., 2019), and chemical methods (Han, J. W.,et al., 2014).

Most commonly, silver nanoparticles (Ag NPs) are used as antimicrobial finishes on functional textiles, making them one of the more commonly encountered nanomaterials (Dastjerdi, R., & Montazer, M., 2010; Chen, X., & Schluesener, H. J., 2008). Antimicrobial qualities aside, these nanoparticles exhibit fascinating optical features. Redox processes benefit greatly from (Kelly, K. L., et al., 2003; Lee, K. S., & El-Sayed, M. A., 2006) and high catalytic activity (Chimentao, R. J., et al., 2004; Pradhan, N., et al., 2002).

Silver nanoparticles (AgNPs) have attracted many researchers owing to their unique physical, chemical, optical, and surface properties. Chemical reduction methods are frequently used to prepare AgNPs, due to their ease of synthesizing them in the solution (Gurunathan, S., et al., 2015). Chemical reduction methods include reducing agents, metal precursors, and stabilizing/capping agents (Gurunathan, S., et al., 2015).

Different applications require different shapes and sizes of AgNPs, which can be tailored to provide the above-mentioned specific features. When using surface-enhanced Raman spectroscopy, it is necessary to activate the nanoparticles by the addition of substances that induce their aggregation or even recrystallization onto particles approximately one order of magnitude larger (Prucek, R., et al., 2011) in order to achieve the high enhancement effect of hundreds of nanometer-sized particles (Michaels, A. M., et al., 1999).

As nanoparticle size decreases, antibacterial activity of Ag NPs rises (Morones, J. R., et al, 2005; Panacek, A., et al., 2014) .Nanoparticles' ability to catalyse reactions is a particularly challenging problem. Silver nanoparticles' catalytic activity is enhanced as the nanoparticle size decreases, with the maximum catalytical activity seen at particle sizes as low as 5 nm in the case

of anthracene catalytic hydrogenation (Deng, J. P., et al., 2007) or even below 1 nm in the case of electrocatalytic reduction of oxygen. (Lu, Y., & Chen, W., 2012)

An inert carrier-anchored AgNP catalyst for the partial oxidation of propylene to propylene oxide and acrolein showed the same reliance on particle size for catalytic activity (Molina, L. M., et al., 2011). However, it was shown that the size of the Ag NPs utilised had an effect on both the catalytic action and the selectivity for propylene oxide formation, with the latter rising with increasing particle size.

Because of the wide range of applications in which Ag NPs are utilised, dependable methods for synthesising nanoparticles of a precise size and form are still being developed. According to this perspective, "wet" preparation methods (chemical reduction of silver salt in solution) predominate (Evanoff Jr, D. D., & Chumanov, G., 2005; Wilcoxon, J. P., & Abrams, B. L., 2006; Tao, A. R., et al., 2008; Guo, S., & Wang, E., 2011).

Silver salt is reduced in a two-step process utilising a strong reducing agent and a lesser reducing agent, resulting in AgNPs with a regulated particle size. This process is known as the "traditional" technique for synthesis of AgNPs with controlled particle sizes (Shirtcliffe, N., et al., 1999; Schneider, S., et al., 1994). It is feasible to make AgNPs ranging in size from 20 to 170 nm using this method, however the consistency of the process appears to be limited.

AgNPs can form hexagonal, spherical, fibers, cubic, prisms, shells (Fahmy, A., et al., 2016), and nanowires (Liz-Marzán, L. M., 2020). Surface plasmon resonance is a phenomenon that characterizes metal nanoparticles (Han, J. W.,et al., 2014). SPR occurs when the incident light excites the metal nanoparticles to generate free conduction electrons. The dimension of metal nanoparticles must be smaller than the incident light wavelength that is the condition for the realization of this phenomenon (Jana, J., et al., 2016; Madami, W., & Seoudi, R., 2020). Based on the shape and size of metal nanoparticles, optical properties have been changed (Nedyalkov, N., et al., 2020; Wang, W., et al., 2018).

Silver nanoparticles combined with organic or inorganic chromophores are more efficient with light than other particles with the same dimension (Oliveira, E., et al., 2015). Polymers can be used as stabilization agents or coating agents with metal nanoparticles to affect the particle

surface atomic structure, preventing the aggregation of nanoparticles (Bhushan, B., et al., 2014; Tommalieh, M. J., et al., 2021).

Polymers are materials that have semi-crystalline or amorphous properties (Ragab, H. M., & Rajeh, A., 2020). There are many studies and applications about metal nanoparticles blended within the polymer to obtain new features that polymer cannot exist alone (Morsi, M. A.,et al., 2018).

The study of metal nanoparticles and dye-doped in the polymer is one of the most attractive fields for scientists due to their optical applications, photodetectors, light-emitting diodes, solar cells, optical sensitivity (Sakhno, O., et al., 2020) and solid-state lasers (Ghosh, D., & Chattopadhyay, N., 2015). Rhodamine B (RhB) is an organic fluorescent dye that can dissolve in water and ethanol because its structures have electron donor and electron acceptor groups (Kazemifard, S., et al., 2018; Sarkar, A., et al., 2019). Moreover, it has fluorescence emitters in the ultraviolet and visible electromagnetic range (Koppal, V. V., et al., 2019).

Fluorescent can be defined as an exciting molecule via light to emit light with a wavelength longer than excited light (Jana, J., et al., 2016). This work aims to improve the emission spectra of the RhB/AgNPs doped polyacrylic acid by adding different sizes and shapes of silver nanoparticles. Silver nanoparticles are prepared with various sizes and in spherical and nanorod shapes with distinct aspect ratios using chemical reduction methods. Based on the results, it can be decided which of these samples increases the fluorescence intensity to be used in an active laser medium.

ISSN-P: 2807-5987

2. Materials and Methods

2.1. Materials

Silver nitrate ($AgNO_3$) purity rating of >99.0%, sodium borohydride ($NaBH_4$) purity rating of 99.99%, tri-sodium citrate ($C_6H_5Na_3O_7$.$2H_2O$) purity rating of ≥ 98%, polyacrylic acid $[C_3H_4O_2]_n$ in powder form, with a molecular weight of 450,000 g/mol, were purchased from Sigma-Aldrich (USA). Rhodamine B ($C_{28}H_{31}ClN_2O_3$) dye content ≥ 95% was purchased from ACROS (USA). Its typical color is pale green to very dark green, and its soluble color is brilliant pink.

2.2 Preparation of AgNPs

Silver nanoparticles were synthesized by dissolved 0.010185 gm of $AgNO_3$ in 600 ml deionized water (D.W) to give a concentration 1mM, and heating at 80 ^{O}C under magnetic stirring, then 0.05295 gm of trisodium citrate to give a concentration 3.4x 10^{-4} M was added, and then 5µl of $NaBH_4$ with a concentration of 1M was added as a reducing agent for the reaction. The mixture changed to a yellow color, indicating the growth of Ag nanoparticles. Just as the color changed, at time T=0 minutes, the sample was removed from the hot plate and left to cool at room temperature. Samples (S1 - S6) were prepared by taking 100 ml from the mixture at different times (t=0.5, 1.0, 3.0, 7.0, 11, 25 minutes), respectively.

2.3. Fabrication of PAA Doped by (RhB/AgNPs) Thin Films

Eight grams of (PAA) (450,000 g/mol) was added to 200 ml (distilled water) to give concentrations 4% under magnetic stirring. The solution of PAA was heated until completely dissolved, at which 5 ml of dissolved PAA was poured on a petri dish (9 cm) to form PAA as a thin film. 0.074901 gm of RhB was dissolved in 100 ml of distilled water under magnetic stirring at room temperature to get RhB solution with a concentration of 1x10^{-3} M. To prepare a dye-doped film from PAA, different quantities of RhB (5×10^{-5}M) and AgNPs were mixed and doped with 5 ml of pure PAA. The mixture was poured on a petri dish (9 cm) and leave at room temperature to form a thin film

ISSN-E: 26632806

2.4. Samples Characterization

The absorbance spectrum of AgNPs colloidal was carried out using the UV-VIS-NIR Spectrometer (Thermo-scientific Evolution 220 Spectrophotometer) at a resolution of 2 nm. The vibrational spectra were carried out using (FTIR) Jasco Model 300E Fourier Transform Infrared Spectrometer. A transmission electron microscope (TEM) was performed to analyze the morphology samples and calculate the particle size; 10 ml of the sample solution was placed on carbon-coated 200 mesh copper grids and allowed to air dry.

TEM of the samples was performed using a JEOL JEM-1100 microscope (JEOL Ltd., Tokyo, Japan) equipped with a tungsten thermionic gun operating at a 100-kV accelerating voltage. TEM images were acquired with a CCD camera. The X-ray diffraction pattern was measured using CuKα radiation at 40 kV and 40 mA, and λ of 1.5406 Å. The scanning was performed over $2\theta^{o}$ range from 30° to 90° at a speed of 0.02°/s. The crystal size of the nanoparticles was calculated using Scherrer's formula. Morphological characterization was carried out by using (SEM) scanning electron microscopy (JSM-6380 LA). The fluorescence spectra were measured using the Jasco FP-777 spectrofluorometer. The light source is a Xenon arc lamp 150 W.

3. Results and Discussion

3.1 UV–Vis Results of Silver Nanoparticles

The UV-visible spectra of Ag nanoparticles were shown in Figure (1). These spectra showed an absorption peak at 408±3 nm for all samples (S1-S6). This band indicates the formation of AgNPs and known as the surface plasmon resonance (SPR). The principle of SPR is the resonance between collective oscillations electrons in AgNPs and the external incident electromagnetic wave (Krasovskii, V. I., & Karavanskii, V. A., 2008; Krajczewski, J., et al., 2017).

The position of the surface plasmon band did not change with heating time. This is probably due to the combination of trisodium citrate and AgNPs, which are based on electronegativity that helps stabilize AgNPs. However, the adsorption intensity of the bands increased with increasing heating time, probably due to the increase in the number of AgNPs in the solution. On the other side, the half bandwidth decreased over time, dropping from 101 nm to 92.6 nm between 0.5 min and 15 min. A higher distribution of AgNPs at a more extended time likely causes this effect.

ISSN-P: 2807-5987

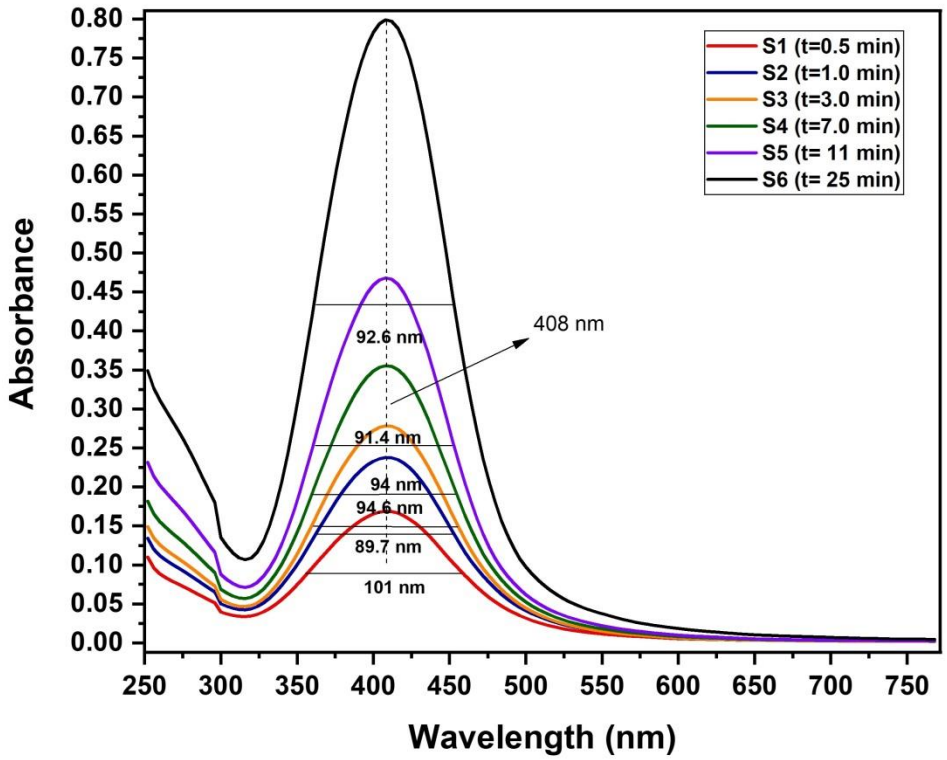

Figure (1): Absorbance spectra of silver nanoparticles synthesized at temperature (80 °C) and at different times.

3.1.1 **UV-Visible of PAA Doped by RhB/AgNPs**

The absorption spectra of PAA doped with an equivalent amount of RhB/AgNPs (13 nm) was shown in figure (2a). The polyacrylic acid (PAA) film is transparent and has no absorption band in the visible range, and RhB has an absorption band at 552 nm due to π-π^* transition as shown inset Figure (2a). However, by adding both AgNPs/RhB, a strong band was found at 560 nm and a low-intensity band at 408 nm. The first band is a sign to RhB, and the second band indicates to AgNPs. The movement of the RhB band (552 nm) to the red-shift (560 nm) may be due to the surface plasmon band of silver nanoparticles interfering with RhB. Moreover, the interaction between AgNPs/RhB molecules changes the electrostatic distribution around RhB and shrinkage of PAA and the smaller distance between AgNPs. This leads to increased aggregation of RhB molecules, resulting in red-shift (Desai, R., et al., 2012).

The intensity of the absorbance band at 560 nm increased with increasing molar concentrations of both AgNPs and RhB due to the greater color intensity in the PAA-doped film. On the other hand, half-bandwidth decreased because PAA contributes to stabilizing AgNPs with RhB. The intensity

ISSN-E: 26632806

of the absorption band PAA-doped by RhB and AgNPs (19 nm) as shown in figure (2b) became weak, possibly due to the lower number of AgNPs distribution.

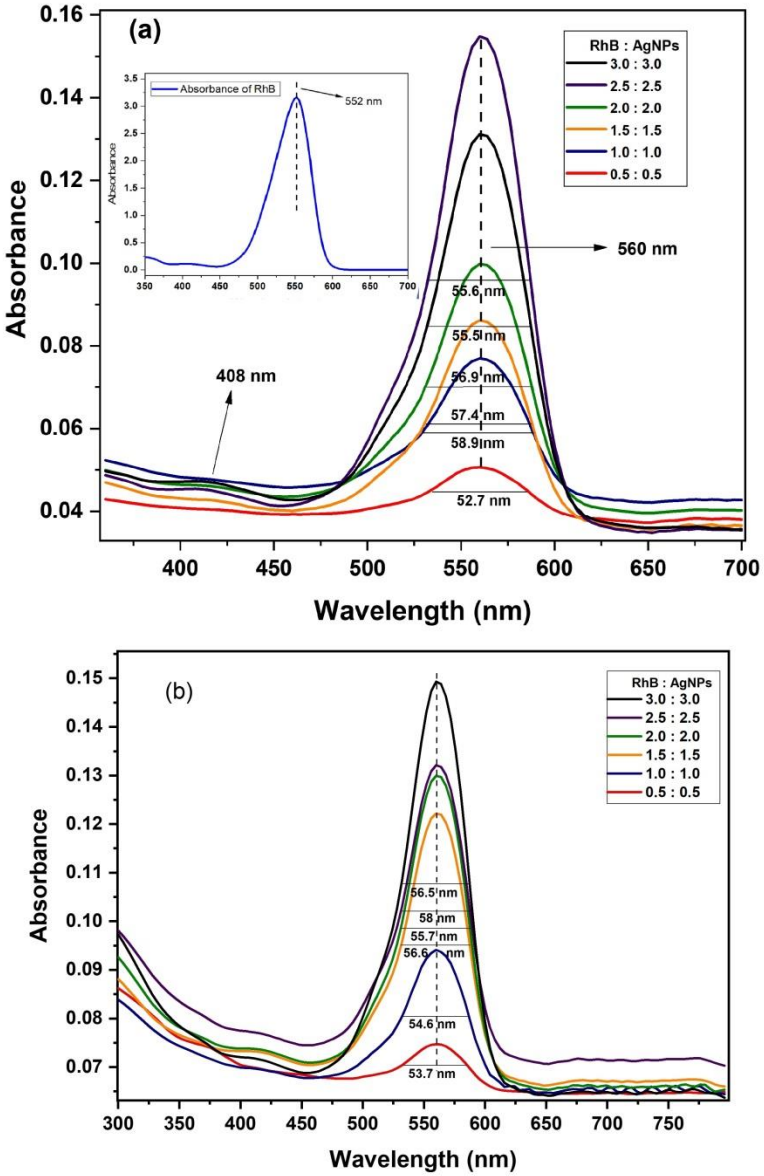

Figure (2a, 2b): Ultraviolet-visible spectra of PAA film doped by equivalent amounts of RhB/AgNPs (13 and 19 nm) with different molar ratios.

3.1.2: FTIR of PAA and PAA Doped by RhB/AgNPs

The FTIR spectra of PAA and PAA doped with RhB/AgNPs (13 nm and 19 nm) was shown in figure (3a, 3b). Two absorbance bands at 3424 $cm^{-1}$and 3349 cm^{-1} in PAA assigned to O-H and –CO(OH) stretching vibrations. These bands changed to 3438 $cm^{-1}$and 3338 cm^{-1} **in the spectra of PAA doped by** RhB/AgNPs **due to the interaction between the –CO (OH) groups**

and AgNPs. The band appeared at 2944 cm^{-1} and interpreted the CH_2 stretching vibration in PAA was unchanged in PAA **doped by RhB/AgNPs**. Moreover, overtone and combination of C-O and C-H groups appearing at 2645 cm^{-1} were unchanged.

Two bands manifest at 1712 $cm^{-1}$and 1689 cm^{-1} equated to C=O stretching vibration in PAA. The disappearance of the second band in the PAA doped proved the interaction between AgNPs and the C=O group. The bending vibration band at 1436 cm^{-1} as a result of C-O-H was broadened in the PAA embedded. The band at 1243 cm^{-1} assigned to the C-O coupled OH bending vibration is the same as in PAA doped. The band at 1197 cm^{-1} in PAA, which was associated with C-O-H groups, transformed to 1199 cm^{-1} in the doped PAA.

The band appearing at 802 cm^{-1} assigned to C-COOH stretching vibration evidence showed no change in the doped PAA. By comparing the spectra for each PAA doped by RhB and AgNPs at two different sizes (13 and 19 nm) as shown in figure (3a, 3b), there is no appreciable change in both except for the difference in intensity. Therefore, all nanoparticles of different sizes were associated with PAA through the C=O group by chemical or electrostatic interaction.

ISSN-P: 2807-5987

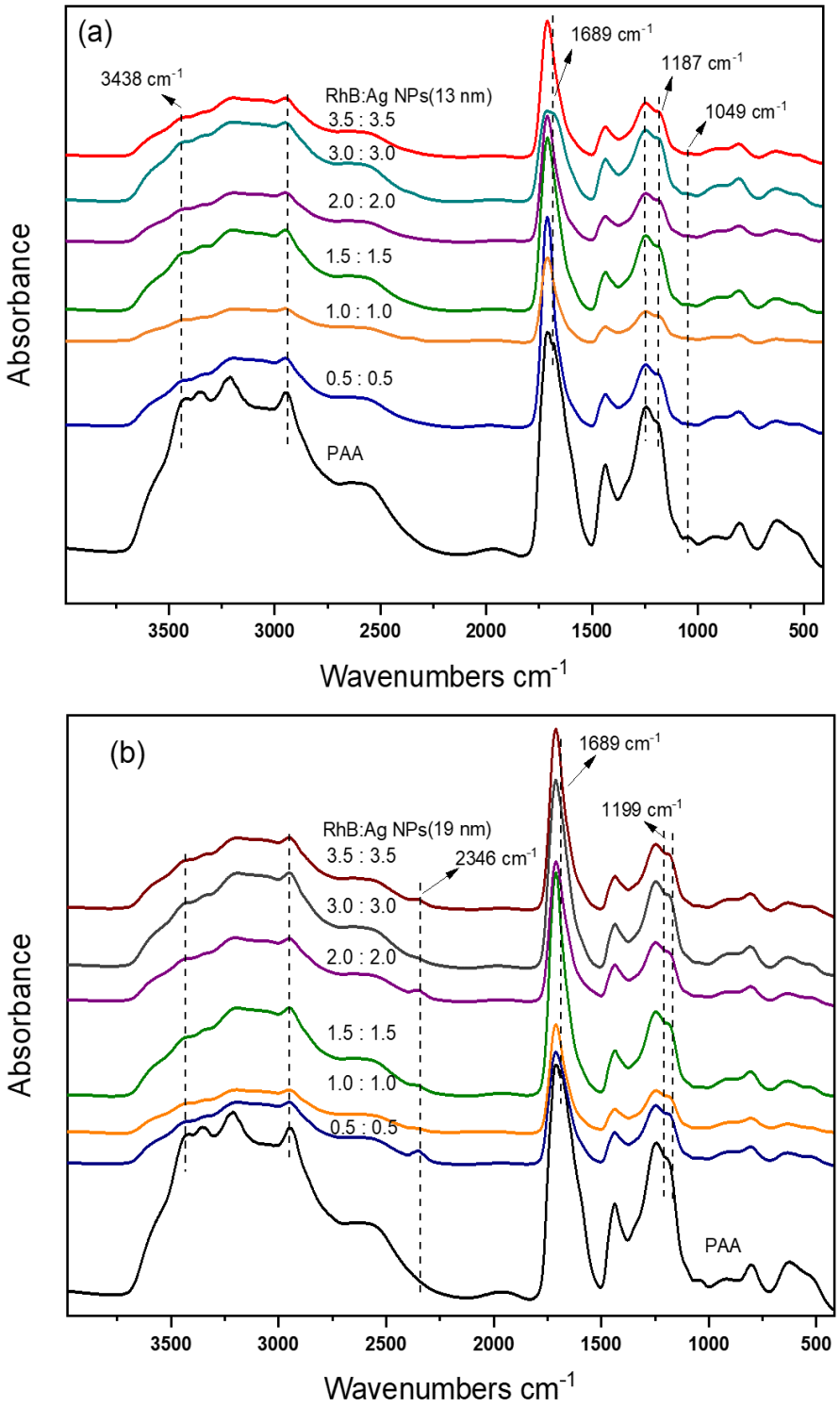

Figure (3a, 3b): Infrared spectra of PAA film doped by equivalent amounts of RhB/AgNPs (13 and 19 nm) with different molar ratios.

ISSN-E: 26632806

ISSN-P: 2807-5987

3.2 TEM of Silver Nanoparticles

Figure (4a) showed that AgNPs prepared at 80 ^{o}C for 1 min. AgNPs appeared as dark spots and are usually spherical in shape, with some prism shapes. The average particle size was determined and found to be 13 nm from the relationship between the repeated particles of the same size in the images (frequency %) and those of different sizes in Figure (4b). TEM images of AgNPs prepared at 80 ^{o}C for 3 min showed that the prepared sample exhibits dark and gray spot sizes with hexagonal, cylindrical, and spherical shapes as shown in Figure (4c). The average particle size was calculated at 19 nm as shown in Figure (4d).

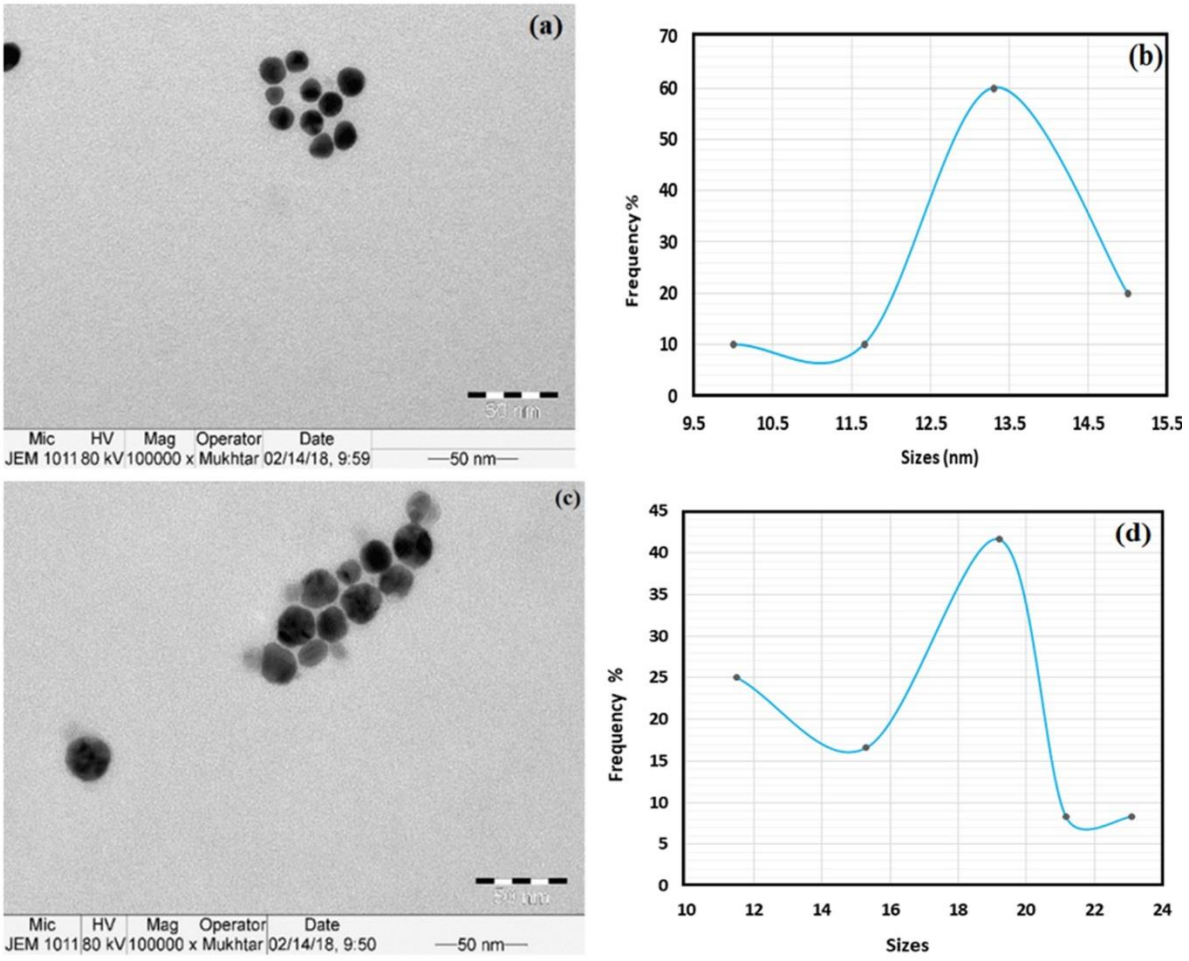

Figure (4): Transmission electron microscopy image of (a) silver nanoparticles prepared at 80 ^{o}C and time 1 min, (b) the frequency % as a function of different particle sizes, (c) silver nanoparticles prepared at 80 ^{o}C and time 3 min, (d) the frequency % as a function of varying particle size.

ISSN-E: 26632806

ISSN-P: 2807-5987

3.3. X-Ray Diffraction of PAA Doped by RhB/AgNPs

Figure (5a, 5b) showed the change in intensity of the x-ray diffraction pattern with 2θ^{o} in the range (30 ^{o} to 85 ^{o}) of PAA doped with the same concentrations of RhB/AgNPs (13 and 19 nm). The diffraction pattern peaks observed at 37.41^{o}, 43.67^{o}, 63.94^{o}, 77^{o}, and 81.23^{o} have different intensities and were matched to (111), (200), (220), (311), and (222) planes, respectively. These results were matched with the data in (International Center for Diffraction Data, JCDS 4-0783) (Bharathi, D., et al., 2018).

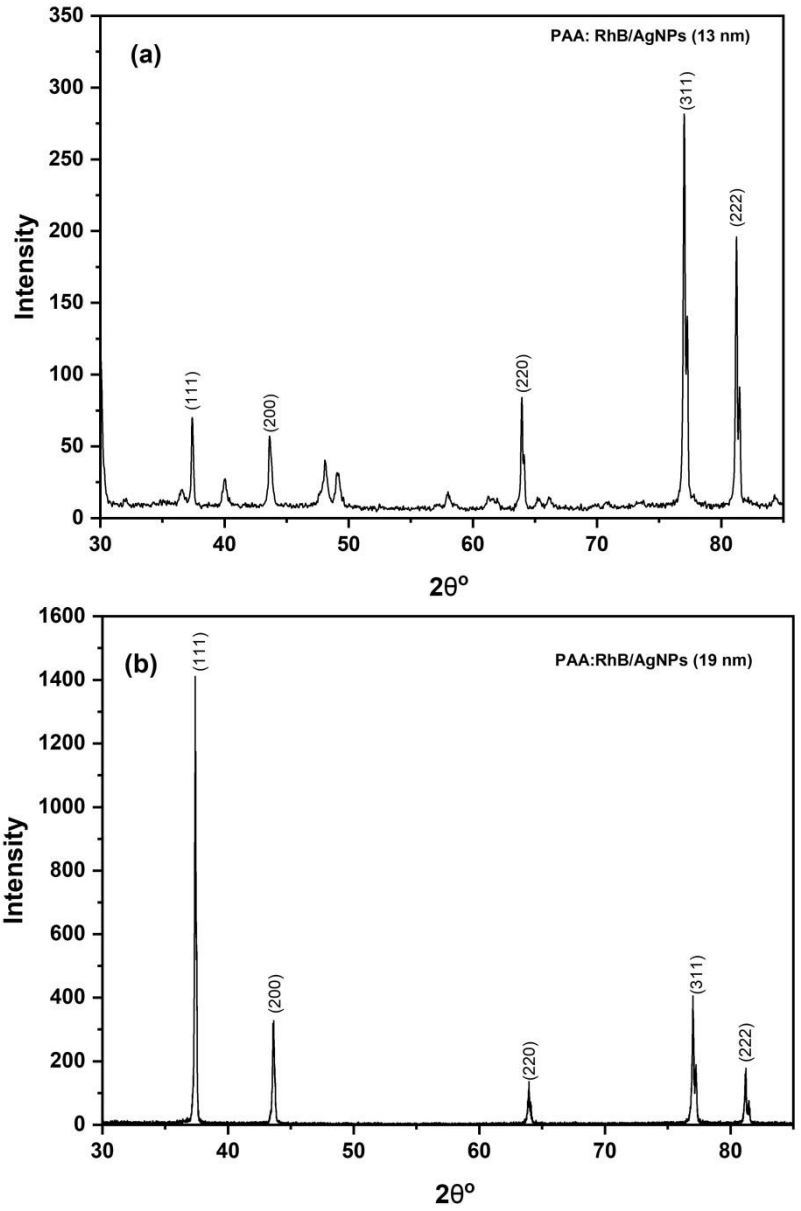

Figure (5): X-ray diffraction pattern of PAA film doped with two equivalent amounts of RhB/AgNPs (a) AgNPs (13 nm) and (b) AgNPs (19 nm).

ISSN-E: 26632806

ISSN-P: 2807-5987

The diffraction pattern was similar to the Braggs reflection of the silver nanoparticle. The results showed that the structure of AgNPs was a face-centered-cubic (fcc) and is in agreement with the previous work of Mollick, et al. (2012).

The crystal sizes at each peak were estimated using Scherrer's formula (Tripathi, J., et al., 2013):

$$D = \frac{0.9\lambda}{\beta \cos \theta} ,$$

where D is the crystal size, θ^o is the Bragg angle, β is the half-bandwidth broadening of the X-ray peak, and λ is the X-ray wavelength (1.540562 A^o).

Crystal sizes of each peak were multiplied by the (intensity peak/maximum intensity). The crystal sizes values at 48 nm, 30 nm, 38 nm, 32 nm, and 57 nm were estimated for the peaks at $2\theta^o$ (37.41^o, 43.67^o, 63.94^o, 77^o, and 81.23^o, and at 48 nm, 42 nm, 43 nm, 31 nm, and 28 nm for the peaks that appeared at $2\theta^o$ (37.38^o, 43.63^o, 63.95^o, 77.01^o, and 81.21^o in PAA doped by RhB/AgNPs (13 and 19 nm) respectively. Thus, the average size calculated for all peaks of the two samples was 41 and 42 nm.

The difference between the average estimated value of crystal size and the value of each peak is due to the difference in the intensity of each peak. The half-bandwidth broadening of the X-ray peaks was inversely proportional to the crystal size of AgNPs. The intensity peaks of PAA doped by AgNPs (13 nm) are lower than that of AgNPs (19 nm) due to attributable particle sizes. Particle sizes calculated from TEM are smaller than those calculated from X-ray. This may be due to the collection of several AgNPs during the preparation of PAA doped by AgNPs/RhB. Additionally, it observed the emergence of Bragg peaks appearing beside the fundamental peaks. These peaks appear for many reasons, including capping agents around AgNPs, as noted by Karthik et al. (2014), or impurities on RhB crystals and an amorphous organic phase seen in the results obtained by Jain and Mehata (2017).

ISSN-P: 2807-5987

3.2 SEM of PAA Doped by RhB/AgNPs

Figure (6a, 6b) shows the scanning electron microscope (SEM) image of PAA film doped with the same values of RhB/AgNPs of two different sizes (13 nm and 19 nm). As shown in Figure (6a) AgNPs with sizes (13 nm) appeared as white spots of different shapes (spherical, popcorn, and cylinder). Furthermore, the particles were randomly distributed in the entire image. The particles are aggregated into PAA and appear as large white particles with various shapes, as shown in Figure (6b) when AgNPs (19 nm) are added to RhB and embedded in PAA.

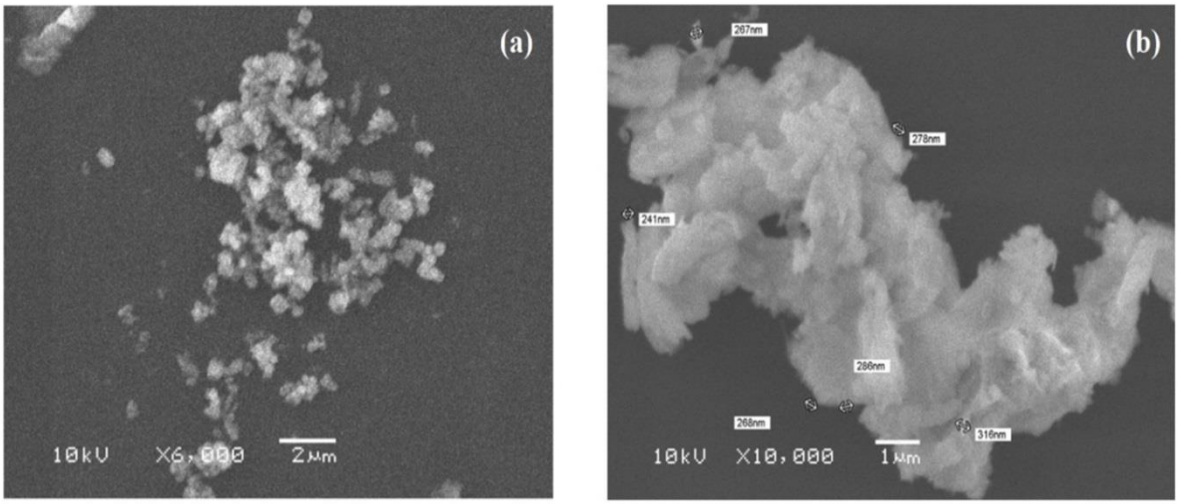

Figure (6): Scanning electron microscope (SEM) images of PAA film doped with two equivalent amounts of RhB/AgNPs (a) AgNPs (13 nm) and (b) AgNPs (19 nm).

By comparing the size of the PAA-doped AgNPs from SEM images and the values calculated in the previous TEM sections of this work, one can see that the particles sizes in the TEM images (13 nm and 19) nm are smaller than those of the post-doping particles. This may be due to some agglomeration was occurred during the preparation of PAA doped with RhB/AgNPs.

ISSN-E: 26632806

3.5: Fluorescence of PAA Doped by RhB/AgNPs

Figure (7) showed the fluorescence spectra of a transparent (PAA) doped with two equivalent amounts of RhB/AgNPs of size (13 and 19 nm) in the range (380 nm–680 nm). The samples were excited at 408 nm (the surface plasmon band of AgNPs discussed in UV-Vis results) to release fluorescent light. The fluorescence bands appeared at 440 nm, 443 nm, 439 nm, 439 nm, 440 nm of PAA doped by different ratios of RhB/AgNPs (13 nm) (1.0: 1.0), (1.5: 1.5), (2.0: 2.0), (2.5: 2.5), and (3.0: 3.0) in Figure (7a), respectively is due to the emission from silver nanoparticles. The bands at 588 nm, 591.5 nm, 585.5 nm, 585.5 nm, and 585 nm of RhB/AgNPs (13 nm) with the ratios above referred to emissions from RhB for PAA doped by RhB/AgNPs (13 nm). The intensity of emissions spectra was increased with an increase in the concentrations of RhB/AgNPs (13 nm). The fluorescence emission that appeared at a higher wavelength was low compared to that at a lower wavelength. This is due to the exciting wavelength of 408 nm (surface plasmon band of AgNPs) having a weak effect on the fluorescence of RhB and a substantial impact on the fluorescence of AgNPs.

The emission bands had no direct linear effect on the molar ratio of AgNPs/RhB (color groups); an increase or decrease in the intensity of emissions can occur with strange behavior. These behaviors agreed with the previous works by Jana et al. (2016) and Paul et al. (2016). The maximum intensity displayed at lower emission band at 440 nm and higher emission band at 590 nm when the molar ratios of AgNPs/ RhB were (2: 2 ml). These ratios indicate an increase in the electric transition among the color-bearing groups in AgNPs/RhB. The intensity of fluorescence tended to decrease at the last ratio (3.0: 3.0 ml) because the PAA film was saturated with silver nanoparticles at that point (Deng, H., & Yu, H., 2018).

From our view, the RhB was assembled on the surface of AgNP and RhB. This leading to a decrease in the fluorescence intensity of AgNPs. One of the most significant characteristics of PAA-doped film is indicated by the Stokes shift formula, which describes the difference in the dipole moments between the ground state (S0) and the first excited state (S1).

$$\nabla\lambda = \lambda_f - \lambda_a \qquad (1)$$

ISSN-P: 2807-5987

where the wavelength λ_f and λ_a is the fluorescence and the absorbance maximum, respectively. The spectral features of the lasing PAA-doped depend on the intermolecular interaction between the RhB/AgNPs and the PAA macromolecules (Chubinidze, K., et al., 2017).

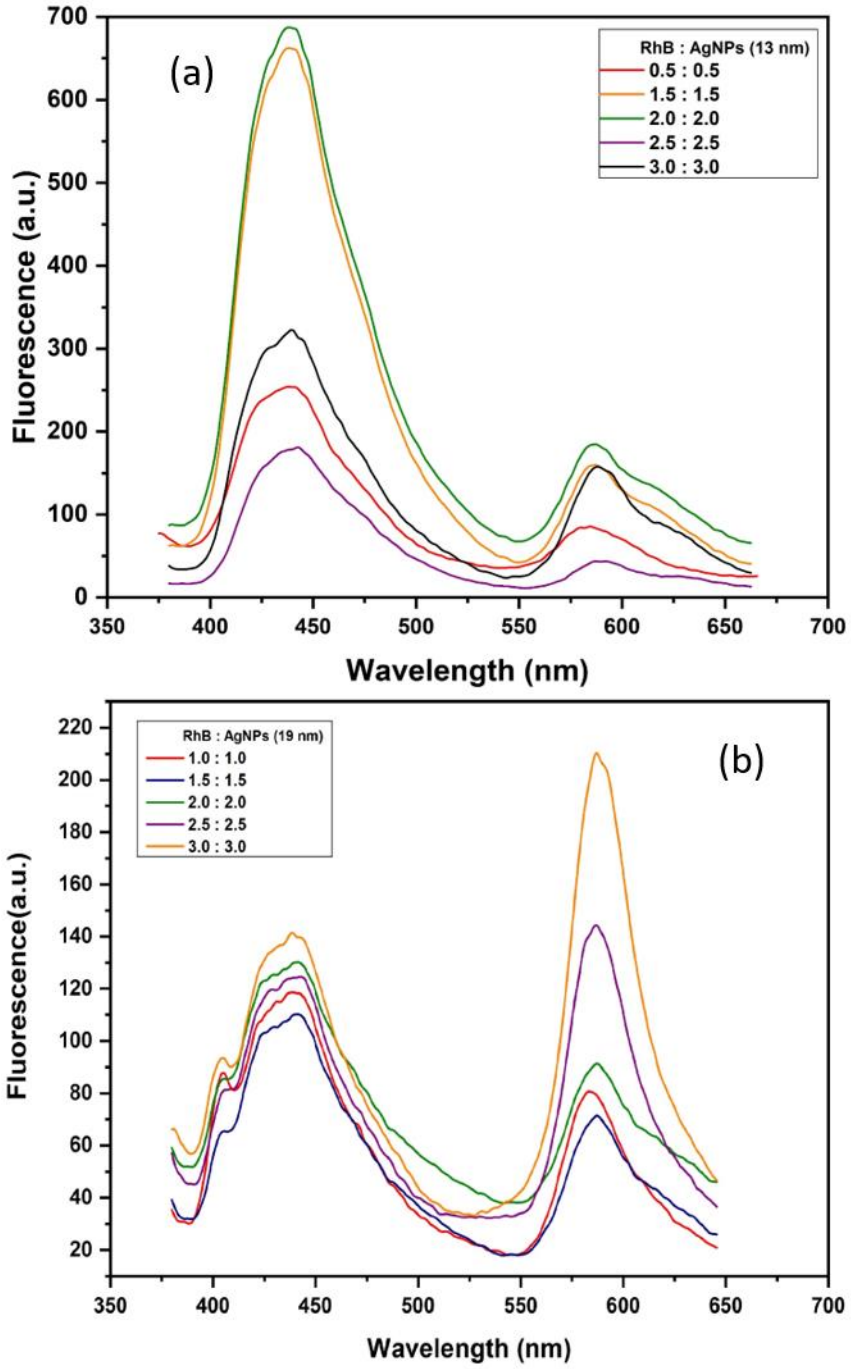

Figure (7a, 7b): Fluorescence spectra of PAA film doped with equivalent amounts of RhB and AgNPs (13 and 19 nm) with different molar ratios

ISSN-E: 26632806

The values of the Stokes shifts were listed in Table 1. The degree of Stokes shift indicated in Table 1 was changed by changing the molar ratio of AgNPs/RhB, suggesting a difference in the self-absorption of the fluorescence between the AgNPs/RhB molecules. The band that appeared at 438 nm in PAA-doped by RhB/AgNPs (19 nm) in Figure (7b) is the fluorescence emission of AgNPs. The emission bands of RhB were appeared at 587 nm, 586.5 nm, 587 nm, 587 nm, and 583 nm of PAA doped by RhB/AgNPs (19 nm) with molar ratios (1.0: 1.0), (1.5: 1.5), (2.0: 2.0), (2.5: 2.5), and (3.0: 3.0) respectively.

Table 1. *Photophysical properties of PAA film with equivalent amounts of RhB and AgNPs (13 and 19 nm) with different molar ratios*

Polymer	**Molar ratio RhB: AgNPs(13nm)**	**Absorption Wavelength (λ_a)**	**Fluorescence wavelength (λ_f)**	$\nabla\lambda = \lambda_f - \lambda_a$
PAA	0.5: 0.5	408 nm	440 nm	32 nm
	1.5: 1.5	408 nm	439 nm	31 nm
	2.0: 2.0	408 nm	439 nm	31 nm
	2.5: 2.5	408 nm	443 nm	35 nm
	3.0: 3.0	408 nm	440 nm	32 nm
Polymer	**Molar ratio RhB: AgNPs (19 nm)**	**Absorption wavelength (λ_a)**	**Fluorescence wavelength (λ_f)**	$\nabla\lambda = \lambda_f - \lambda_a$
PAA	1.0 :1.0	408 nm	438 nm	30 nm
	1.5: 1.5	408 nm	438 nm	30 nm
	2.0 : 2.0	408 nm	438 nm	30 nm
	2.5: 2.5	408 nm	438 nm	30 nm
	3.0 : 3.0	408 nm	438 nm	30 nm

There is no linear relationship between fluorescence intensity and the molar ratio of AgNPs/RhB doped in PAA (Paul, B., et al., 2016). There was no apparent shift in emission bands. Comparing these results with those presented at AgNPs (13 nm), it can note that the fluorescence spectra intensity of AgNPs/RhB has decreased due to more aggregation of nanoparticles, leading to the accumulation of RhB, and thus to the low fluorescence intensity. The maximum absorbance intensity was noted in the molar ratio of AgNPs/RhB at (3.0: 3.0). This is due to the color-bearing groups of RhB and the electric transition between AgNPs and RhB, the molecules (Deng, H., & Yu, H., 2018).

One can observe from the degree of Stokes shift captured in Table 1 that increasing the molar ratio of AgNPs/RhB led to a steady rate of self-absorption for the fluorescence spectrum via the AgNPs (19 nm) and RhB molecules. The differences in the fluorescence between PAA doped (RhB/AgNPs (13 nm) and PAA doped (RhB/AgNPs (19 nm) can be accounted for by the strong interaction between AgNPs/RhB, which occurs due to the proximity of AgNPs and RhB.

4. Conclusion

Silver nanoparticles (AgNPs) with different particles sizes were prepared by chemical reduction method. Two bands at 560 nm and 408 nm in UV-visible spectra of PAA doped by RhB/AgNPs were assigned to RhB and AgNPs. The two bands that appeared at 1683 $cm^{-1,}$ and 1243 cm^{-1} in FTIR spectra attributed to both C=O and C-O of PAA were shifted due to the electrostatic interaction between AgNPs and PAA through C=O and C-O functional groups.

The TEM results confirmed the formation of AgNPs with spherical shapes. X-ray diffraction showed the crystalline structure of PAA doped by RhB/AgNPs, and crystal sizes were calculated using the Scherrer equation. SEM results demonstrate the particle sizes for AgNPs doped in PAA are larger than those calculated from the TEM images due to the aggregation of nanoparticles during their incorporation into PAA. The fluorescence spectra of PAA doped by RhB/AgNPs (13 nm and 19 nm) at different molar ratios were measured and revealing emission bands at 587 nm and 440 nm for RhB and AgNPs, respectively.

The higher bands were explained by the electronic transition from surface plasmon resonance of the AgNPs and π-π^* of RhB to PAA. Therefore, it can be inferred that AgNPs/RhB doped in PAA film enhanced the fluorescence spectra, which means that these samples can be used for lasers dye enhancement.

5. References

Bharathi, D., Diviya Josebin, M., Vasantharaj, S., & Bhuvaneshwari, V. (2018). Biosynthesis of silver nanoparticles using stem bark extracts of Diospyros montana and their antioxidant and antibacterial activities. *Journal of Nanostructure in Chemistry*, *8*(1), 83-92.

Bhushan, B., Luo, D., Schricker, S. R., Sigmund, W., & Zauscher, S. (Eds.). (2014). *Handbook of nanomaterials properties*. Springer Science & Business Media.

Chen, X., & Schluesener, H. J. (2008). Nanosilver: a nanoproduct in medical application. *Toxicology letters*, *176*(1), 1-12.

Chimentao, R. J., Kirm, I., Medina, F., Rodriguez, X., Cesteros, Y., Salagre, P., & Sueiras, J. E. (2004). Different morphologies of silver nanoparticles as catalysts for the selective oxidation of styrene in the gas phase. *Chemical communications*, (7), 846-847.

Chubinidze, K., Partsvania, B., Devadze, L., Zurabishvili, T., Sepashvili, N., Petriashvili, G., & Chubinidze, M. (2017). Gold nanoparticle conjugated organic dye nanocomposite based photostimulated luminescent enhancement and its application in nanomedicine. *American Journal of Nano Research and Applications*, *5*(3-1), 42-47.

Dastjerdi, R., & Montazer, M. (2010). A review on the application of inorganic nano-structured materials in the modification of textiles: focus on anti-microbial properties. *Colloids and surfaces B: Biointerfaces*, *79*(1), 5-18.

Deng, H., & Yu, H. (2018). Self-assembly of rhodamine 6G on silver nanoparticles. *Chemical Physics Letters*, *692*, 75-80.

Deng, J. P., Shih, W. C., & Mou, C. Y. (2007). Electron transfer-induced hydrogenation of anthracene catalyzed by gold and silver nanoparticles. *The Journal of Physical Chemistry C*, *111*(27), 9723-9728.

Desai, R., Mankad, V., Gupta, S. K., & Jha, P. K. (2012). Size distribution of silver nanoparticles: UV-visible spectroscopic assessment. *Nanoscience and nanotechnology letters*, *4*(1), 30-34.

Evanoff Jr, D. D., & Chumanov, G. (2005). Synthesis and optical properties of silver nanoparticles and arrays. *ChemPhysChem*, *6*(7), 1221-1231.

Fahmy, A., Eisa, W. H., Yosef, M., & Hassan, A. (2016). Ultra-thin films of poly (acrylic acid)/silver nanocomposite coatings for antimicrobial applications. J Spectroscopy 1: 11.

Ghosh, D., & Chattopadhyay, N. (2015). Gold and silver nanoparticles based superquenching of fluorescence: A review. *Journal of Luminescence*, *160*, 223-232.

Gudikandula, K., & Charya Maringanti, S. (2016). Synthesis of silver nanoparticles by chemical and biological methods and their antimicrobial properties. *Journal of Experimental Nanoscience*, *11*(9), 714-721.

Guo, S., & Wang, E. (2011). Noble metal nanomaterials: controllable synthesis and application in fuel cells and analytical sensors. *Nano today*, *6*(3), 240-264.

Gurunathan, S., Jeong, J. K., Han, J. W., Zhang, X. F., Park, J. H., & Kim, J. H. (2015). Multidimensional effects of biologically synthesized silver nanoparticles in Helicobacter pylori, Helicobacter felis, and human lung (L132) and lung carcinoma A549 cells. *Nanoscale research letters*, *10*(1), 1-17.

Han, J. W., Gurunathan, S., Jeong, J. K., Choi, Y. J., Kwon, D. N., Park, J. K., & Kim, J. H. (2014). Oxidative stress mediated cytotoxicity of biologically synthesized silver nanoparticles in human lung epithelial adenocarcinoma cell line. *Nanoscale Research Letters*, *9*(1), 1-14.

Jain, S., & Mehata, M. S. (2017). Medicinal plant leaf extract and pure flavonoid mediated green synthesis of silver nanoparticles and their enhanced antibacterial property. *Scientific reports*, *7*(1), 1-13.

Jana, J., Ganguly, M., & Pal, T. (2016). Enlightening surface plasmon resonance effect of metal nanoparticles for practical spectroscopic application. *RSC advances*, *6*(89), 86174-86211.

Karthik, L., Kumar, G., Kirthi, A. V., Rahuman, A. A., & Bhaskara Rao, K. V. (2014). Streptomyces sp. LK3 mediated synthesis of silver nanoparticles and its biomedical application. *Bioprocess and biosystems engineering*, *37*(2), 261-267.

Kazemifard, S., Naji, L., & Taromi, F. A. (2018). Enhancing the photovoltaic performance of bulk heterojunction polymer solar cells by adding Rhodamine B laser dye as co-sensitizer. *Journal of colloid and interface science*, *515*, 139-151.

Kelly, K. L., Coronado, E., Zhao, L. L., & Schatz, G. C. (2003). The optical properties of metal nanoparticles: the influence of size, shape, and dielectric environment. *The Journal of Physical Chemistry B*, *107*(3), 668-677.

Koppal, V. V., Patil, P. G., Melavanki, R. M., Kusanur, R. A., Afi, U. O., & Patil, N. R. (2019). Exploring the influence of silver nanoparticles on the mechanism of fluorescence quenching of coumarin dye using FRET. *Journal of Molecular Liquids*, *292*, 111419.

Krajczewski, J., Kołątaj, K., & Kudelski, A. (2017). Plasmonic nanoparticles in chemical analysis. *RSC advances*, *7*(28), 17559-17576.

Krasovskii, V. I., & Karavanskii, V. A. (2008). Surface plasmon resonance of metal nanoparticles for interface characterization. *Optical Memory and Neural Networks*, *17*(1), 8-14.

Lee, K. S., & El-Sayed, M. A. (2006). Gold and silver nanoparticles in sensing and imaging: sensitivity of plasmon response to size, shape, and metal composition. *The Journal of Physical Chemistry B*, *110*(39), 19220-19225.

Liz-Marzán, L. M. (2020). Nanometals: formation and color. In *Colloidal Synthesis of Plasmonic Nanometals* (pp. 1-13). Jenny Stanford Publishing.

Lu, Y., & Chen, W. (2012). Size effect of silver nanoclusters on their catalytic activity for oxygen electro-reduction. *Journal of Power Sources*, *197*, 107-110.

Madami, W., & Seoudi, R. (2020). Molecular and fluorescence spectroscopic studies of polyacrylic acid blended with rhodamine B mixed gold nanoparticles. *Journal of Taibah University for Science*, *14*(1), 790-799.

Michaels, A. M., Nirmal, M., & Brus, L. E. (1999). Surface enhanced Raman spectroscopy of individual rhodamine 6G molecules on large Ag nanocrystals. *Journal of the American Chemical Society*, *121*(43), 9932-9939.

Molina, L. M., Lee, S., Sell, K., Barcaro, G., Fortunelli, A., Lee, B., Seifert, S., Winans, R.E., Elam, J.W., Pellin, M.J., Barke, I., & Vajda, S. (2011). Size-dependent selectivity and activity of silver nanoclusters in the partial oxidation of propylene to propylene oxide and acrolein: A joint experimental and theoretical study. *Catalysis today*, *160*(1), 116-130.

Mollick, M. M. R., Bhowmick, B., Maity, D., Mondal, D., Bain, M. K., Bankura, K., Sarkar, J., Rana, D., Acharya, K. & Chattopadhyay, D. (2012). Green synthesis of silver nanoparticles using Paederia foetida L. leaf extract and assessment of their antimicrobial activities. *International Journal of Green Nanotechnology*, *4*(3), 230-239.

Morones, J. R., Elechiguerra, J. L., Camacho, A., Holt, K., Kouri, J. B., Ramírez, J. T., & Yacaman, M. J. (2005). The bactericidal effect of silver nanoparticles. *Nanotechnology*, *16*(10), 2346.

Morsi, M. A., El-Khodary, S. A., & Rajeh, A. (2018). Enhancement of the optical, thermal and electrical properties of PEO/PAM: Li polymer electrolyte films doped with Ag nanoparticles. *Physica B: Condensed Matter*, *539*, 88-96.

Nedyalkov, N., Dikovska, A., Koleva, M., Stankova, N., Nikov, R., Borisova, E., Genova, T., Aleksandrov, L., Iordanova, R.& Terakawa, M. (2020). Luminescence properties of laser-induced silver clusters in borosilicate glass. *Optical Materials*, *100*, 109618.

Ning, S., Wu, Z., Dong, H., Ma, L., Jiao, B., Ding, L., & Zhang, F. (2016). The enhanced random lasing from dye-doped polymer films with different-sized silver nanoparticles. *Organic Electronics*, *30*, 165-170.

Oliveira, E., Núñez, C., Santos, H. M., Fernández-Lodeiro, J., Fernández-Lodeiro, A., Capelo, J. L., & Lodeiro, C. (2015). Revisiting the use of gold and silver functionalised nanoparticles as colorimetric and fluorometric chemosensors for metal ions. *Sensors and Actuators B: Chemical*, *212*, 297-328.

Panacek, A., Prucek, R., Hrbac, J., Nevečná, T. J., Steffkova, J., Zboril, R., & Kvitek, L. (2014). Polyacrylate-assisted size control of silver nanoparticles and their catalytic activity. *Chemistry of materials*, *26*(3), 1332-1339.

Paul, B., Bhuyan, B., Purkayastha, D. D., & Dhar, S. S. (2016). Photocatalytic and antibacterial activities of gold and silver nanoparticles synthesized using biomass of Parkia roxburghii leaf. *Journal of Photochemistry and Photobiology B: Biology*, *154*, 1-7.

Pradhan, N., Pal, A., & Pal, T. (2002). Silver nanoparticle catalyzed reduction of aromatic nitro compounds. *Colloids and Surfaces A: Physicochemical and Engineering Aspects*, *196*(2-3), 247-257.

Prakash, A., Pathrose, B. P., Nampoori, V. P. N., Radhakrishnan, P., & Mujeeb, A. (2019). Thermal diffusivity of neutral red dye using dual beam thermal lens technique: A comparison on the effects using nano pulsed laser ablated silver and gold nanoparticles. *Physica E: Low-dimensional Systems and Nanostructures*, *107*, 203-208.

Prucek, R., Panáček, A., Fargašová, A., Ranc, V., Mašek, V., Kvítek, L., & Zbořil, R. (2011). Re-crystallization of silver nanoparticles in a highly concentrated NaCl environment—a new substrate for surface enhanced IR-visible Raman spectroscopy. *CrystEngComm*, *13*(7), 2242-2248.

Ragab, H. M., & Rajeh, A. (2020). Structural, thermal, optical and conductive properties of PAM/PVA polymer composite doped with Ag nanoparticles for electrochemical application. *Journal of Materials Science: Materials in Electronics*, *31*(19), 16780-16792.

Sakhno, O., Yezhov, P., Hryn, V., Rudenko, V., & Smirnova, T. (2020). Optical and nonlinear properties of photonic polymer nanocomposites and holographic gratings modified with noble metal nanoparticles. *Polymers*, *12*(2), 480.

Sarkar, A., Venkataraj, R., Nampoori, V. P. N., & Kailasnath, M. (2019). Silver nanoparticles filled hollow polymer fiber laser with enhanced photostability. *Optics & Laser Technology*, *112*, 255-260.

Schneider, S., Halbig, P., Grau, H., & Nickel, U. (1994). Reproducible preparation of silver sols with uniform particle size for application in surface-enhanced Raman spectroscopy. *Photochemistry and photobiology*, *60*(6), 605-610.

Shirtcliffe, N., Nickel, U., & Schneider, S. (1999). Reproducible preparation of silver sols with small particle size using borohydride reduction: for use as nuclei for preparation of larger particles. *Journal of colloid and interface science*, *211*(1), 122-129.

Tao, A. R., Habas, S., & Yang, P. (2008). Shape control of colloidal metal nanocrystals. *small*, *4*(3), 310-325.

Tommalieh, M. J., Awwad, N. S., Ibrahium, H. A., & Menazea, A. A. (2021). Characterization and electrical enhancement of PVP/PVA matrix doped by gold nanoparticles prepared by laser ablation. *Radiation Physics and Chemistry*, *179*, 109195.

Tripathi, J., Tripathi, S., Keller, J. M., Das, K., & Shripathi, T. (2013). Degradation study on structural and optical properties of annealed Rhodamine B doped poly (vinyl) alcohol films. *Polymer degradation and stability*, *98*(1), 12-21.

Wang, H., Qiao, X., Chen, J., & Ding, S. (2005). Preparation of silver nanoparticles by chemical reduction method. *Colloids and Surfaces A: Physicochemical and Engineering Aspects*, *256*(2-3), 111-115.

Wang, W., Ramezani, M., Väkeväinen, A. I., Törmä, P., Rivas, J. G., & Odom, T. W. (2018). The rich photonic world of plasmonic nanoparticle arrays. *Materials today*, *21*(3), 303-314.

Wilcoxon, J. P., & Abrams, B. L. (2006). Synthesis, structure and properties of metal nanoclusters. *Chemical Society Reviews*, *35*(11), 1162-1194.